Inhibition of protein arginine deiminase II suppresses retinoblastoma in orthotopic transplantation in mice

SOJIN KIM[1,2*], YONG KEUN SONG[3*], CHANG SIK CHO[4], HYO JUNG KIM[5], SUNGSOON FANG[6], DONG HYUN JO[5] and HYUNKYUNG KIM[1,2]

[1]Department of Biochemistry and Molecular Biology; [2]BK21 Graduate Program, Department of Biomedical Sciences, Korea University College of Medicine, Seoul 02841; [3]Department of Medicine, Seoul National University College of Medicine; [4]Fight against Angiogenesis-Related Blindness Laboratory, Biomedical Research Institute, Seoul National University Hospital; [5]Department of Anatomy and Cell Biology, Seoul National University College of Medicine, Seoul 03080; [6]Severance Biomedical Science Institute, Gangnam Severance Hospital; Graduate School of Medical Science, Brain Korea 21 Project, Yonsei University College of Medicine, Seoul 06273, Republic of Korea

Received November 8, 2022; Accepted February 9, 2023

DOI: 10.3892/or.2023.8583

Abstract. Chemotherapies are used for treating retinoblastoma; however, numerous patients suffer from recurrence or symptoms due to chemotherapy, which emphasizes the need for alternative therapeutic strategies. The present study demonstrated that protein arginine deiminase II (PADI2) was highly expressed in human and mouse retinoblastoma tissues due to the overexpression of E2 factor (E2F). By inhibiting PADI2 activity, the expression of phosphorylated AKT was reduced, and cleaved poly (ADP-ribose) polymerase level was increased, leading to induced apoptosis. Similar results were obtained in orthotopic mouse models with reduced tumor volumes. In addition, BB-Cl-amidine showed low toxicity *in vivo*. These results suggested that PADI2 inhibition has potential clinical translation. Furthermore, the present study highlights the potential of epigenetic approaches to target RB1-deficient mutations at the molecular level. The current findings provide new insights into the importance of retinoblastoma intervention by managing PADI2 activity according to the treatment of specific inhibitors and depletion approaches *in vitro* and in orthotopic mouse models.

Correspondence to: Dr Dong Hyun Jo, Department of Anatomy and Cell Biology, Seoul National University College of Medicine, 103 Daehak-ro, Jongno, Seoul 03080, Republic of Korea
E-mail: lawrenc2@snu.ac.kr

Dr Hyunkyung Kim, Department of Biochemistry and Molecular Biology, Korea University College of Medicine, 73 Goryeodae-ro, Seongbuk, Seoul 02841, Republic of Korea
E-mail: hyunkkim@korea.ac.kr

*Contributed equally

Key words: retinoblastoma, protein arginine deiminase II, BB-Cl-amidine, E2 factor, AKT phosphorylation

Introduction

Retinoblastoma is a malignant ocular tumor that occurs during childhood. Over 95% of the tumors have mutated *RB1*, which is located on chromosome 13 (1). This leads to the deficiency of protein retinoblastoma (pRb), the translational product of the *RB1* gene, which regulates the G_1 checkpoint of the cell cycle by binding to E2 factor (E2F) (2). Therefore, loss of pRb leads to unregulated cell cycle progression, reduced apoptosis and uncontrolled cell proliferation (2,3). Several chemotherapies, radiotherapies and thermotherapies have been used to treat retinoblastoma (4-6). However, numerous patients experience recurrence or symptoms related to the toxicity of chemotherapies, and enucleation is still often implemented, which significantly affects the quality of life after operation (4). Therefore, an alternative therapeutic strategy is imperative to enhance the eye salvation rate and quality of life in young patients.

The translational product of RB1, pRb, binds to E2F and inhibits cell cycle progressive activities. Therefore, deficiency of pRb leads to overexpression and hyperactivity of E2F, which is also known to interact functionally with specificity factor 1 (Sp1) (7,8). The C- terminal domain of Sp1 binds to the N-terminus of E2F, which facilitates its activities (7). Another study has also reported cooperative relations between these two proteins in *Drosophila* and mice (9). An increase in Sp1 can lead to increased expression and activity of protein arginine deiminase II (PADI2) (10,11). A previous study on human keratinocytes reported that Sp1 was involved in regulating PADI2, and that the activity and binding of Sp1 facilitated the transcription of PADI2 (10). Another study reported that Sp1 facilitated the mRNA expression of PADI2 in bone marrow cells in rheumatoid arthritis (11). Therefore, it can be deduced that an increase in Sp1 can lead to overexpression of PADI2. Since E2F activity is known to be increased in retinoblastoma due to RB1 deficiency, this implies that PADI2 may also be overexpressed.

The epigenetic regulator PADI2 is involved in the transcription of genes that accelerate cell proliferation, and is

overexpressed in numerous cancer types, including breast, skin and ovarian cancer (12-15). PADI2 citrullinates the arginine of histone H3, which leads to increased transcription of cell cycle-progressing genes such as RNA polymerase II (16). Previous clinical studies have reported a significant association between PADI2 level and survival (15,17). Furthermore, preclinical studies have reported tumor-suppressive effects of PADI2 inhibition (13,17-20).

Based on the RB1 deficient characteristics of retinoblastoma and previous studies on the role of PADI2 in numerous tumors, it was hypothesized that this may be a novel therapeutic target in retinoblastoma. The present is a preclinical study on the PADI2 inhibitor BB-Cl-amidine in *in vitro* and *in vivo* models of retinoblastoma. Representative cell lines and orthotopic xenograft mouse models were used to evaluate the efficacy and toxicity of BB-Cl-amidine. The results revealed that PADI2 expression was upregulated in retinoblastoma, and PADI2 inhibition attenuated oncogenic activity. These results suggested therapeutic potential and promising prospects for further clinical translation.

Materials and methods

Drugs. BB-Cl-amidine (cat. no. HY-111347A) was purchased from MedChemExpress, while E2F inhibitor (cat. no. 324461) was purchased from Sigma-Aldrich; Merck KGaA.

Cell lines. Two retinoblastoma cell lines, Y79 and WERI-Rb-1, were used in the present study. Y79 [cat. no. HTB-18; American Type Culture Collection (ATCC)] and WERI-Rb-1 (cat. no. HTB-169; ATCC) cells were cultured in RPMI-1640 medium (cat. no. 30-2001; ATCC and cat. no. LM011-01; Welgene, Inc.) at 37˚C with 5% CO_2. A normal retinal pigment epithelium cell line, ARPE-19, was used for comparison. ARPE-19 (cat. no. CRL-2302; ATCC) cells were cultured in DMEM-F12 medium (cat. no. 30-2006; ATCC and cat. no. LM002-04; Welgene, Inc.).

Orthotopic xenograft mouse model. An orthotopic retinoblastoma mouse model was generated by injecting cultivated Y79 and WERI-Rb-1 cell lines into the vitreous cavity of BALB/c-nude mice (OrientBio Inc.) according to previous protocols (21,22). All animal experiments were performed with the approval (approval no. SNU-220512-3) of the Institutional Research Ethics Committee of Seoul National University College (Seoul, Korea). All mice were 6-weeks old female. A total of 20 mice were used with an average weight of 20 g. They were kept in cages with individual circulation. The temperature was controlled in the range of 20-25˚C. Remaining food and water were monitored daily and refilled whenever needed. The light/dark cycle was 14/10 h according to the institution's guideline. The health conditions and behavior of all animals were monitored 5 times a week with professional veterinarian assistance. The number of mice per standard cage was restricted to 5 mice according to the institution's animal ethics guideline. Cells at a density of $2x10^4$ cells per eye were suspended in PBS. Prior to intravitreal cell injection, mice were put under complete anesthesia to minimize suffering and distress. They were also placed under infrared lighting to prevent hypothermia when under anesthesia and were monitored carefully until full conscious was confirmed. For anesthesia, Zoletil (30 mg/kg; Virbac) and xylazine (10 mg/kg; Bayer-Korea, Ltd.) were injected intraperitoneally according to a previous protocol (23). A previous publication supported the use of Zoletil for anesthetic purposes (24). After adequate anesthesia, the cell suspension was injected into one eye per mouse using a 30-gauge needle. Control group and an experimental group which received BB-Cl-amidine injection consisted of 10 mice. BB-Cl-amidine (2 μM) was injected intravitreally following the anesthesia 2 weeks after the injection of cells. All mice were euthanized, visually graded and enucleated 4 weeks after cell injection, making the total duration of 4 weeks. It was planned to euthanize any mice that exhibited ≥15% loss of body weight, or showed protruded eyeball. However, no mouse was succumbed or reached humane endpoints during the duration of the experiment. When the pre-planned termination timepoint was reached, all mice were first anesthesized with the same protocol implemented before intravitreal injection. After full unconsciousness was confirmed, mice were placed in a CO_2 chamber where they were sacrificed by a flow rate of CO_2 that caused 50% displacement of the cage volume per min. This took place at January 2022. Animal death was confirmed by 20 min of observation of full unconsciousness and absence of breathing and heartbeat. All procedures followed the guidelines of the National Institutes of Health for euthanasia of rodents. Mice were maintained and treated in a specific-pathogen-free facility, in accordance with the Association for Research in Vision and Ophthalmology statement for the use of animals in ophthalmic and vision research.

pLKO.1 lentiviral infection. The lentiviral pLKO.1 vector-small hairpin RNA (shRNA) based on a 2nd generation system targeting PADI2 (shPADI2), and negative control (shNS) were supplied by Yonsei University. The following shRNA sequences were used: shNS, 5'-CCGGCAACAAGA TGAAGAGCACCAACTCGAGTTGGTGCTCTTCATCTT GTTGTTTTT-3'; shPADI2 (1), 5'-GCACCTTCATCGACG ACATTT-3'; and shPADI2 (2), 5'-GTGTGCTGCATGAAG GATAAT-3'. To generate stable transfectants, 293T cells were seeded in 60-mm plates and the 1 μg lentiviral pLKO.1 vector and virus packing mixture (including 750 ng psPAX2 packaging plasmid and 250 ng pMD2.G envelope plasmid) were co-transfected into 293T cells (cat. no. CRL-1573; ATCC) with Polyethylenimine (PEI, cat. no. 408727; Sigma-Aldrich; Merck KGaA) for 24 h at 37˚C. 293T cells were changed with fresh medium and incubated for 48 h at 37˚C. Next, the virus-containing medium was harvested and concentrated using a lenti-X concentrator (cat. no. 631231; Takara Bio, Inc.) according to the manufacturer's instructions. A total of 5 ml of lentivirus-containing medium and 1.5 ml of a concentrator were mixed, incubated for 30 min at 37˚C, and centrifuged by 1,500 x g for 45 min at 4˚C in a centrifuge (cat. no. 1248R; LABOGENE). After removing the supernatant, the viral pellet was resuspended in fresh medium and added to Y79 cells seeded in 60-mm plates without dilution for lentiviral transduction. The multiplicity of infection (MOI) value was not defined. Culture scales of the packaging cells and the target cells were the same, and the virus obtained from one plate of 293T infected one plate of Y79 cells. The shRNA-transduced Y79 cells were incubated for 24 h at 37˚C. After 24 h, the

medium was replaced with fresh medium containing 1 μg/ml puromycin (cat. no. P8833; Sigma-Aldrich; Merck KGaA). Puromycin-resistant clones were selected. Knockdown efficiency was evaluated using western blotting.

Reverse transcription PCR (RT-PCR). Y79 cells were seeded in 60-mm plates at a density of $1x10^6$ cells and treated with E2F inhibitor 40 μM. After treating E2F inhibitor for 0, 24 and 48 h, the cells were harvested. Following harvest, total RNA was extracted using QIAzol Lysis Reagent (cat. no. 79306; Qiagen, Inc.) according to the manufacturer's instructions. Total RNA concentration was measured using a NanoDrop 2000 spectrophotometer (NanoDrop Technologies; Thermo Fisher Scientific, Inc.) at a wavelength of 260 nm. Total RNA (1,000 ng) was reverse transcribed to cDNA using amfiRivert cDNA Synthesis Platinum Master Mix (cat. no. R5600; GenDEPOT, LLC) at 42˚C for 1 h, and the reaction was quenched by heating at 94˚C for 5 min. RT-PCR was performed using Takara PCR Thermal Cycler Dice (cat. no. TP600; Takara Bio, Inc.). cDNA (1 μl) was amplified with 2.5 U *Pfu* polymerase, 50 mM KCl, 10 mM Tris-HCl (pH 8.3), 1.5 mM $MgCl_2$, 0.02 mM dNTPs (cat. no. E-2015-1; Bioneer Corporation) and 0.1 μM each primer. The following primer sequences were used: PADI2 forward, 5'-ACAAAGTGGGCG TGTTCTACG-3' and reverse, 5'-CCACCCGTGTACTTGACC A-3'; and HPRT forward, 5'-TGACACTGGCAAAACAAT GCA-3' and reverse, 5'-GGTCCTTTTCACCAGCAAGCT-3'. The PCR products were electrophoresed on 2% agarose gels at 100 V for 30 min. The HPRT was used as internal control for normalization. The PCR products were electrophoresed on 2% agarose gels containing SafePinky DNA Gel staining solution (cat. no. S1001-025; GenDEPOT, LLC) at 100 V for 30 min. The agarose gel was exposed and the bands were visualized using Gel Doc™ XR system (cat. no. 170-8170; BIO-RAD, Inc.).

Cell proliferation assay. Y79 and ARPE-19 cells were seeded in 96-well plates at a density of $5x10^3$ cells per well and treated with DMSO or different concentrations of BB-Cl-amidine (0.5, 1, 1.5, 2 and 2.5 μM) for 48 h. Subsequently, 20 μl MTS reagent (cat. no. G3580; Promega Corporation) was added to each well, and the cells were incubated at 37˚C for 1 h in the dark. Finally, the quantity of the formazan product was measured by recording the absorbance at 490 nm using a 96-well plate reader (cat. no. 340PC384; Molecular Devices, LLC).

Cell counting and colony formation assay. For the cell counting assay, Y79 cells were seeded in 12-well plates at a density of $1x10^5$ cells/well. The cells were treated with DMSO or BB-Cl-amidine (2 μM), harvested, and counted at 0, 24, 48 and 72 h after treatment. Each counting was performed eight times, and the mean was obtained.

For the colony formation assay, Y79 cells were seeded in 12-well plates coated with 100 mg/ml poly-D-lysine (cat. no. A38904-01; Gibco; Thermo Fisher Scientific, Inc.) at a density of $1x10^3$ cells per well and treated with DMSO or BB-Cl-amidine (2 μM). The cells were then incubated at 37˚C for 2 weeks. After forming colonies, the colonies were washed twice with PBS, fixed with 100% methanol for 10 min, stained with 1% crystal violet for 30 min, and washed with distilled water. Finally, the images of colonies were captured, and the colonies were counted using the ImageJ 1.53K software (National Institutes of Health).

Immunofluorescence assay. Y79 cells were plated on a 12-well plate coated with poly-D-lysine and incubated at 37˚C for 48 h. For inhibition of PADI2, Y79 cells were treated with BB-Cl-amidine 2 μM or small hairpin RNA (shRNA). Subsequently, the cells were fixed with 4% paraformaldehyde at room temperature for 10 min and permeabilized with 0.1% Triton X-100 for 5 min. Next, the cells were treated with 2% bovine serum albumin (BSA, cat. no. A0100-010; GenDEPOT, LLC) for 1 h to minimize nonspecific binding and then incubated with primary antibodies in 2% BSA at 4˚C overnight. The next day, the cells were treated with Alexa Fluor 488 goat IgG antibody (cat. no. A-11034; Thermo Fisher Scientific, Inc.) in 2% BSA (1:1,000) at room temperature for 1 h. Nuclear staining was performed using DAPI solution (cat. no. 62248; Thermo Fisher Scientific, Inc.). Finally, the slips were observed under a fluorescence microscope (EVOS™ FL Auto 2 Imaging system, cat. no. AMAFD2000; Thermo Fisher Scientific, Inc.). The primary antibodies used were against Ki67 (1:500; cat. no. ab15580; Abcam) and BrdU (1:500; cat. no. 11296736001; Roche Diagnostics).

Wound healing assay. Y79 cells were cultured overnight in 12-well plates coated with poly-D-lysine. After Y79 cells were 100% of confluency, straight wounds were created using 200-μl pipette tips. Next, straight wounds were created using 200-μl pipette tips. After washing with culture medium to remove cell debris, the wounded cells were incubated in medium with 10% FBS (cat. no. F0900-050; GenDEPOT, LLC) containing DMSO or BB-Cl-amidine (2 μM). Images of the wound gaps were captured at 0, 24, 48 and 72 h. The results were evaluated using an EVOS microscope (cat. no. AMAFD2000; Thermo Fisher Scientific, Inc.).

Invasion assay. Transwell inserts (24-well plate; pore size 8.0 μM; cat. no. 37224; SPL Life Sciences) were coated with 100 μg/ml fibronectin (cat. no. F2006; Sigma) for 1 h. The upper surface of the Transwell insert was then coated with 100 μl Matrigel diluted 1:5 in serum-free RPMI-1640 medium at 37˚C overnight. Y79 cells were seeded at a density of $1x10^5$ cells per well in the upper chamber with 200 μl serum-free medium and treated with DMSO or BB-Cl-amidine (2 μM). The bottom chamber was filled with 800 μl complete medium containing 10% FBS (cat. no. F0900-050; GenDEPOT, LLC). After 36 h, the invasive cells were fixed with 100% methanol for 10 min and stained with 1% crystal violet at room temperature for 10 min. Finally, images of the Transwell inserts were captured using an EVOS microscope (cat. no. AMAFD2000; Thermo Fisher Scientific, Inc.) at x20 magnification. The migration assay was performed similarly to the invasion assay, with the exception of the Transwell inserts, which were not coated with Matrigel.

Western blot assay. Upon harvesting, cells were lysed in lysis buffer [50 mM Tris-HCl (pH 8.0), 200 mM NaCl and 0.5% NP-40] containing a protease inhibitor cocktail (cat. no. 11836153001; Sigma-Aldrich; Merck KGaA) for

30 min on ice. The lysates were centrifuged at 15,000 x g at 4˚C for 15 min and the supernatants were collected. Total protein was quantified by BCA assay (cat. no. 23227; Thermo Fisher Scientific, Inc.). Total protein (~20 μg) was separated by 10-14% SDS-PAGE and transferred to a PVDF membrane (cat. no. 1620177; Bio-Rad Laboratories, Inc.). The membranes were blocked in Tris-buffered saline containing 0.1% Tween 20 and 5% skim milk (cat. no. CNS109; CELLNEST) at room temperature for 30 min, and incubated with primary at 4˚C for overnight and secondary antibodies at room temperature for 1 h. The signal was visualized using an enhanced chemiluminescence detection system (cat. no. W3652-020; GenDEPOT, LLC). The band intensities were calculated using the ImageJ 1.53K software (National Institutes of Health).

The following primary antibodies were used: Anti-β-actin (1:3,000; cat. no. A5441; Sigma-Aldrich; Merck KGaA), anti-PADI2 (1:1,000; cat. no. 12110-1-AP; Proteintech Group, Inc.) anti-cleaved poly (ADP-ribose) polymerase (PARP) (1:1,000; cat. no. 5625), anti-AKT (1:1,000; cat. no. 9272) and anti-phosphorylated (p)-AKT (1:1,000; cat. no. 9271; all from Cell Signaling Technology, Inc.). The HRP-conjugated AffiniPure Goat Anti-Rabbit IgG (H + L) and HRP-conjugated AffiniPure Goat Anti-Mouse IgG (H + L) secondary antibodies were as follows: (1:3,000-5,000; cat. nos. 111-035-003 and 115-035-003; Jackson ImmunoResearch Laboratories, Inc.). In addition, the b-actin was used as a loading control for normalization.

Cell apoptosis assay. Cell apoptosis assay was performed using Annexin V-FITC Apoptosis Kit (cat. no. K101-100; BioVision, Inc.). Cells were treated with DMSO or different concentrations of BB-Cl-amidine (1 and 2 μM). After washing with PBS, the harvested cells were resuspended in 500 μl 1X binding buffer and 5 μl annexin V-FITC, propidium iodide (PI), or both at room temperature for 5 min in the dark. Finally, early (annexin V-FITC$^+$/PI$^-$) and late (annexin V-FITC$^+$/PI$^+$) apoptosis was measured by flow cytometric analysis (BD FACSCanto II; BD Biosciences) and BD FlowJo software (v.10.8.1; FlowJo LLC).

Additionally, Apopxin Green Indicator staining assay was performed using Apoptosis/Necrosis Assay Kit (cat. no. ab176749; Abcam). Cells were seeded in 12-well plates and treated with DMSO or different concentrations of BB-Cl-amidine (0.5 and 1 μM) at a density of 5x10^4 cells per well. After 48 h, the cells were prepared and treated according to the manufacturer's protocol. Images of apoptotic (green, GFP channel) and viable cells (blue, DAPI channel) were captured using a fluorescence microscope (EVOS-FL; Thermo Fisher Scientific, Inc.).

Cell cycle assay (PI staining assay). Cell cycle assay was performed with PI staining. Briefly, cells were treated with DMSO or BB-Cl-amidine (2 μM) for 48 h and harvested. The harvested cells were washed and fixed. Next, 200 μl RNase (1 mg/ml; cat. no. 12091021; Thermo Fisher Scientific, Inc.) was added. The samples were incubated at 37˚C for 30 min and stained with 300 μl PI solution (50 mg/ml in PBS; cat. no. P4170; Sigma-Aldrich; Merck KGaA) in the dark. Finally, the cell cycle was measured by flow cytometric analysis (BD FACSCanto II and BD FlowJo software v.10.8.1).

Visual grading of tumor. A visual grading system for evaluating tumor formation was used. Following sacrifice, the eyes were evaluated according to the preset grading system and images were obtained for further review. The grading system consists of grades 0 to 5, and the standards were elaborated by our group, as previously described in a previous study (25).

Immunofluorescence of mouse tissue. The enucleated eyeballs of mice were formalin-fixed, embedded in paraffin blocks, sectioned (4 μm) and deparaffinized with Shandon Xylene Substitute (cat. no. 6764506; Epredia). The sections were then stained with a primary antibody against PADI2 (cat. no. 12110-1-AP; Proteintech Group, Inc.) overnight at 4˚C according to the manufacturer's protocols. After overnight incubation, Alexa Fluor 594-attached antibody (1:400; cat. no. A-11012; Invitrogen; Thermo Fisher scientific, Inc.) was used as a secondary antibody. The results were evaluated by fluorescence microscopy (Eclipse 90i; Nikon Corporation).

Human tissue microarray. Human retinoblastoma tissue slides, including 24 retinoblastoma tissues originated from 12 different donors (cat. no. BV35111a; Biomax). Immunostaining of the purchased slides was performed as aforementioned with tissue from mice, using the same antibodies and observing the results under a fluorescence microscope. The slides were stained with hematoxylin and eosin (H&E) for histological analysis and comparison. H&E slides were scanned and analyzed using an Aperio ImageScope x64 (Leica Microsystems, Inc.).

Toxicity evaluation. Mice (6-week-old C57BL/6; Koatech) were intravitreally injected with 2 μM BB-Cl-amidine after general anesthesia. Optomotor response measurement (OptoMotry HD; CerebralMechanics) and electroretinography (cat. no. UTAS E-2000; LKC Technologies) were performed 1 week after injection according to previous guidelines (26). Enucleated eyes were prepared and analyzed using H&E staining and TUNEL assay. Structure and toxicity evaluations were performed according to a previously established protocol (22). The results of H&E staining were analyzed by measuring the a/b ratio, where 'a' is the length from the innermost ganglion cell layer to the outermost inner nuclear layer, while 'b' is the length from the innermost ganglion cell layer to the outermost outer nuclear layer. All mice were maintained in a specific-pathogen free facility as previously described, in accordance with the ARVO statement.

Statistical analysis. Data from the visual grading of tumors were statistically analyzed using the U-Mann Whitney test (27,28). The results of the cell viability, colony formation, wound healing and apoptosis assays were analyzed via one-way ANOVA with post-hoc Bonferroni's test. The results of the cell proliferation assay were analyzed by comparing the control and BB-Cl-amidine groups at different time points with unpaired Student's t-test. Quantification of BrdU, and Ki67 staining was also performed with unpaired Student's t-test. The proportion of cell cycle status was analyzed using two-way ANOVA with post-hoc Bonferroni's test. All statistical analyses were performed using GraphPad Prism version 9 (GraphPad Software; Inc.).

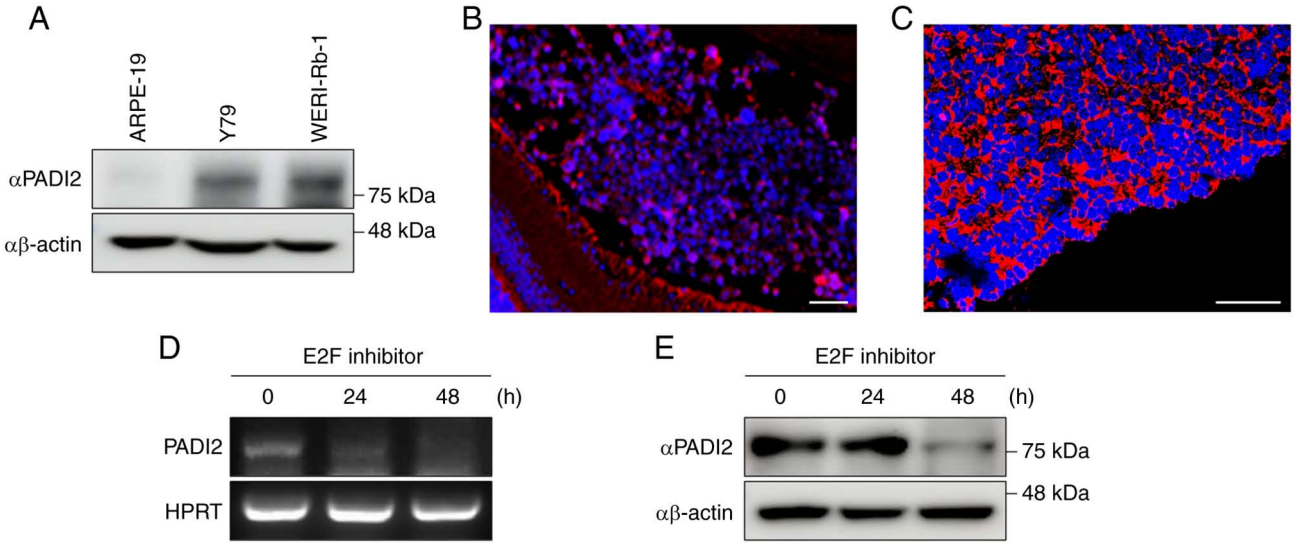

Figure 1. PADI2 is highly expressed in retinoblastoma, and E2F inhibition induces PADI2 overexpression. (A) Protein expression level of PADI2 in the human retinoblastoma cell lines Y79 and WERI-Rb-1 compared with that in the human retinal pigment epithelial cell line ARPE-19, as determined by western blotting. (B and C) Expression of PADI2 in (B) orthotopic retinoblastoma tissue of mouse (magnification, x200) and (C) human retinoblastoma tissue (magnification, x400), as determined by immunostaining assay. Scale bar, 50 μm. (D and E) mRNA and protein expression levels of PADI2 after treatment with an E2F inhibitor (40 μM) for 0, 24 and 48 h, as determined by (D) reverse transcription PCR and (E) western blotting. PADI2, protein arginine deiminase II; E2F, E2 factor.

Results

PADI2 is highly expressed in retinoblastoma and RB1 mutation induces PADI2 overexpression. The protein expression of PADI2 in ARPE-19, Y79 and WERI-Rb-1 cells was first evaluated. Western blotting showed that PADI2 protein was highly expressed in the retinoblastoma cell lines Y79 and WERI-Rb-1 compared with that in human retinal pigment epithelium ARPE-19 cells (Fig. 1A). Immunohistochemistry performed on retinoblastoma and normal retina tissue indicated that the expression of PADI2 was upregulated in both mouse and human retinoblastoma tissues (Figs. 1B and C, and S1A). A distinct difference in expression of PADI2 was observed between the retina of normal mice and orthotopic retinoblastoma tissue (Figs. 1B and S1A). The expression of PADI2 was also elevated in human retinoblastoma tissue (Fig. 1C).

A previous study reported that Sp1-binding sites were highly present in the PADI2 promoter (10). Indeed, E2F becomes free when it is not bound to pRb, which is absent in retinoblastoma cells due to RB1 gene mutation, and interacts with Sp1 which results in elevation of both proteins (7-9). Elevated Sp1 then interacts with PADI2 promoter. Therefore, it was hypothesized that free E2F may regulate the expression of PADI2 in retinoblastoma with mutated RB1. To confirm this hypothesis, the mRNA and protein expression of PADI2 was confirmed by treatment with an E2F inhibitor. It was found that the expression of PADI2 was downregulated when cells were treated with an E2F inhibitor for 48 h (Fig. 1D and E), and that PADI2 was aberrantly expressed in retinoblastoma.

PADI2 inhibition suppresses proliferation and regulates phosphorylated (p)-AKT expression in vitro. The present study aimed to determine the role of PADI2 in retinoblastoma. To confirm whether PADI2 affected the viability of Y79 cells, the effects of BB-Cl-amidine (a small molecule inhibitor of PADI2) were evaluated in Y79 and ARPE-19 cells. Cells were treated with DMSO and BB-Cl-amidine for 48 h, and MTS assay was performed. The results revealed that BB-Cl-amidine reduced the viability of Y79 cells in a dose-dependent manner (Fig. 2A); however, ARPE-19 cells were not affected (Fig. 2B). These results demonstrated that PADI2 inhibition explicitly attenuated the viability of the aforementioned retinoblastoma cell line.

Next, changes in cell proliferation were analyzed to investigate whether inhibition of PADI2 regulated the proliferation of Y79 cells. When BB-Cl-amidine was treated time-dependently, Y79 cells did not proliferate compared with control cells (Fig. 2C). Furthermore, PADI2 in Y79 cells was depleted using a lentiviral system to determine whether PADI2 knockdown had similar effects to BB-Cl-amidine treatment. PADI2-depleted Y79 cells proliferated more slowly than control cells (Fig. 2D). The fluorescence intensity of BrdU and Ki67 (cell proliferation markers) was also evaluated. The results showed that BrdU incorporation and Ki67 levels effectively decreased in BB-Cl-amidine-treated Y79 cells (Figs. 2E and S2A). In addition, Ki67 staining was performed in PADI2-knockdown Y79 cells, indicating that PADI2 ablation inhibited cancer cell growth (Fig. 2F). To further evaluate the oncogenic role of PADI2 in retinoblastoma, colony formation, invasion and wound healing assays were performed following BB-Cl-amidine treatment and PADI2 depletion. PADI2 inhibition reduced colony formation (Fig. 2G and H), invasiveness (Fig. S2B) and wound healing activity (Fig. S2C) in Y79 cells.

Furthermore, it was hypothesized that the molecular mechanism of PADI2 involves cell proliferation and invasion. AKT kinase regulates cell proliferation and survival in numerous human cancer types, including retinoblastoma, and breast, colorectal and prostate cancer (29-35). p-AKT regulates tumorigenesis and metastasis in breast cancer (30),

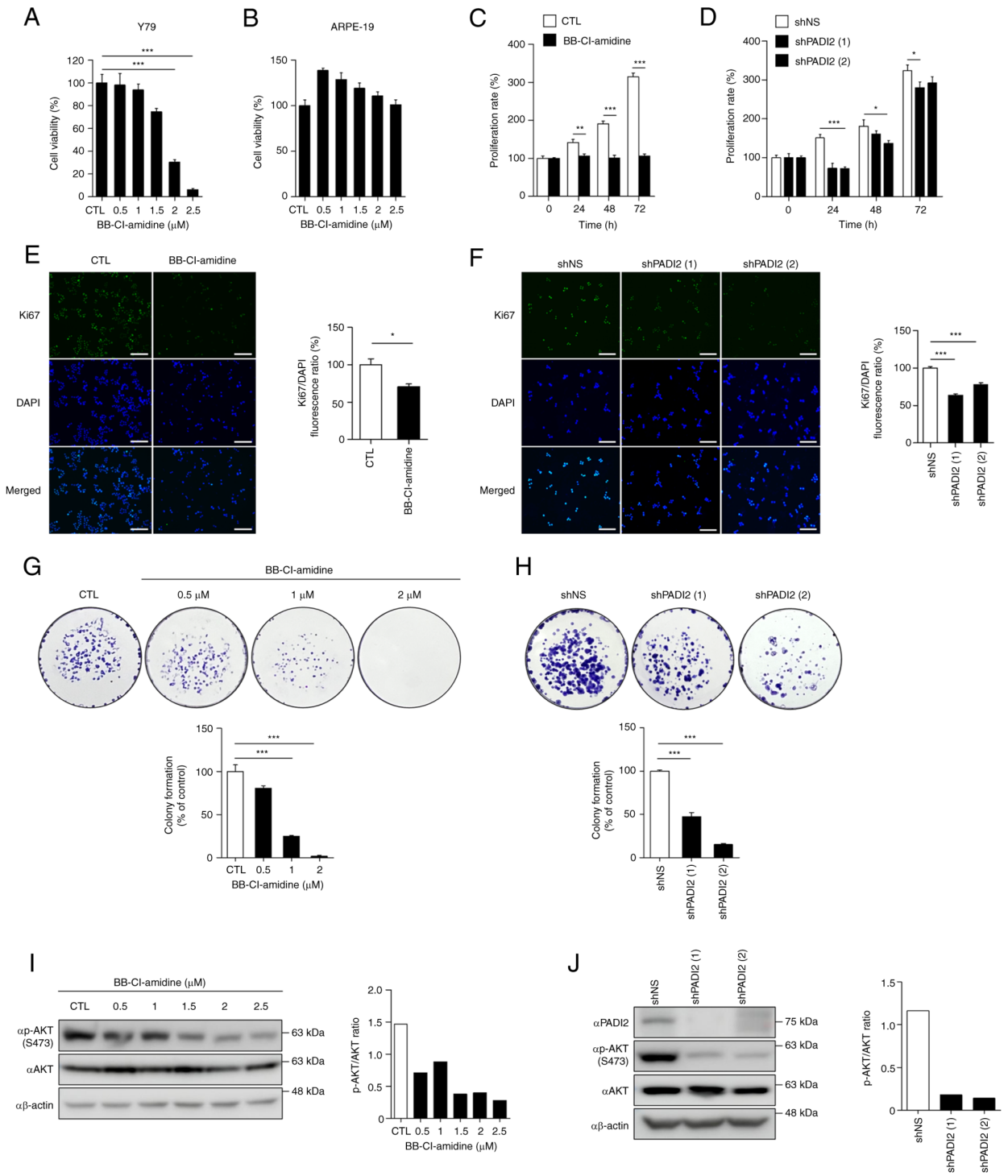

Figure 2. PADI2 inhibition suppresses proliferation and regulates p-AKT expression *in vitro*. (A and B) Cell viability of (A) Y79 and (B) ARPE-19 cells treated with BB-Cl-amidine (a small molecule inhibitor of PADI2) for 48 h in a dose-dependent manner by MTS assay (n=4). (C and D) Proliferation rates of (C) Y79 cells treated with DMSO and 2 μM BB-Cl-amidine (n=8) or (D) control and PADI2-depleted Y79 cells in a time-dependent manner, as determined by cell counting assay (n=4). (E and F) Fluorescence intensity of the proliferation marker Ki67 in (E) Y79 cells treated with DMSO and 2 μM BB-Cl-amidine for 48 h (n=3) or (F) control and PADI2-depleted Y79 cells, as determined by immunofluorescence assay (n=4). Representative immunostaining images (left) and graphs of the Ki67/DAPI fluorescence ratio (right) are shown (magnification, x20). Scale bar, 125 μm. (G and H) Quantitative analysis of colony formation in (G) Y79 cells treated with DMSO and BB-Cl-amidine (n=3) or (H) control and PADI2-depleted Y79 cells for 2 weeks (n=4). Representative images of colony formation (top) and graphs of colony formation (% of control) (bottom) are shown. (I and J) Protein expression of PADI2, p-AKT and AKT in (I) Y79 cells treated with DMSO and BB-Cl-amidine for 48 h or (J) control and PADI2-depleted Y79 cells, as determined by western blotting. Western blotting images (left) and graphs of the P-AKT/AKT ratio (right) are shown. Bars indicate SEM. *P≤0.05, **P≤0.01 and ***P≤0.001, as determined by (A and F-H) one-way ANOVA with post-hoc Bonferroni test, (C and D) two-way ANOVA with post-hoc Bonferroni test or (E) unpaired Student's t-test. PADI2, protein arginine deiminase II; p-, phosphorylated.

and elevated p-AKT activity increases tumor progression and invasiveness in prostate cancer expressing low levels of PTEN (31). In addition, inhibition of methyltransferase-like 3 induces apoptotic cell death via the PI3K/AKT/mTOR

signaling pathway (34), and oncogenes such as tribbles pseudokinase 3 and ribosome biogenesis regulator 1 homolog promote cell proliferation and invasion via the AKT/mTOR signaling pathway in retinoblastoma (33,35). Therefore, it is crucial to identify targets that control the AKT signaling pathway in cancer. As revealed in Fig. 2I, the p-AKT levels gradually decreased in BB-Cl-amidine-treated Y79 cells. When p-AKT expression in PADI2-depleted Y79 cells was confirmed, the p-AKT level was reduced compared with that in the control cells (Fig. 2J). Thus, PADI2 regulated p-AKT expression, thereby enhancing cancer cell proliferation.

PADI2 inhibition induces cancer cell death in vitro. Next, cancer cell death induced by PADI2 suppression was verified in Y79 cells. PARP belongs to the NAD^+ ADP-ribosyl transferase family, which is essential for the metabolism of various biological processes and is involved in apoptosis (36). Treatment of Y79 cells with BB-Cl-amidine increased the level of cleaved PARP in a dose-dependent manner (Fig. 3A). This result was also observed in PADI2-knockdown Y79 cells (Fig. 3B). In addition, it was found that the expression of cleaved PARP was elevated in WERI-Rb-1 cells following BB-Cl-amidine treatment (Fig. S3A). These results indicated that both BB-Cl-amidine and PADI2 elimination had pro-apoptotic effects in retinoblastoma cells.

Additional cell death analyses were performed, including the Apopxin Green Indicator staining, annexin V-FITC assay and cell cycle analysis. As demonstrated in Fig. 3C, the fluorescence intensity of the apoptotic phosphatidylserine sensor Apopxin Green was significantly enhanced after treatment with BB-Cl-amidine in Y79 cells. When WERI-Rb-1 cells were treated with BB-Cl-amidine, similar result as in Y79 cells were confirmed (Fig. S3B). As the concentration of BB-Cl-amidine increased, a greater percentage of sub-G1 population was observed (Fig. 3D). Furthermore, flow cytometric analysis of annexin V revealed a similar tendency under BB-Cl-amidine treatment in Y79 cells (Fig. 3E). When PADI2 shRNA was introduced, the sub-G1 population and annexin V staining pattern were consistent with those of PADI2 inhibitor treatment (Fig. 3F and G). Taken together, these data suggested that PADI2 inhibition effectively induced cancer cell death.

PADI2 inhibition suppresses tumor growth in vivo. Orthotopic transplantation mouse models were used to examine the *in vivo* effects of PADI2 inhibition. PADI2 inhibition was performed with either shRNA introduction or BB-Cl-amidine injection. Two weeks after intravitreally injecting the representative retinoblastoma cell lines Y79 and WERI-Rb-1, BB-Cl-amidine was administered intravitreally at a dosage of 2 μM, in parallel to the *in vitro* assays. PBS, the solvent of BB-Cl-amidine, was injected into the control groups. The size of the tumors was evaluated after 2 weeks, immediately after euthanasia, according to previously described standards of grade (21,25) (Fig. 4A). The mean grade of the groups injected with the PADI2 inhibitor was significantly lower than that of the control in both Y79 and WERI-Rb-1-injected mice. This indicated that inhibition of PADI2 suppressed tumor growth *in vivo*. In addition, tumors of grade 5 did not occur in PADI2-inhibited eyes (Fig. 4B and C). Representative images of H&E staining in each group also showed histological differences caused by PADI2 inhibition (Fig. 4B and C). After 4 weeks, tumors transfected with PADI2 shRNA were evaluated using the same protocols (21,25), and were compared with control mice (which were injected with Y79 cells) without PADI2 shRNA transfection. Tumors originating from PADI2-depleted retinoblastoma cells showed attenuated growth, similar to the results obtained with BB-Cl-amidine (Fig. 4D). Collectively, these data demonstrated that PADI2 inhibition suppressed tumor growth in retinoblastoma mouse models.

BB-Cl-amidine has a low-toxicity profile. To assess its potential for clinical translation, the toxicity profile of the PADI2 inhibitor BB-Cl-amidine was investigated. Optomotor response measurement and electroretinography were used to assess the optical function, while H&E staining and TUNEL assay were used for histological examination. In total, 3 mice were injected with BB-Cl-amidine in one eye and PBS in the other eye for comparison. There was no significant difference in optomotor response between the two groups, indicating no definite toxic effects on visual function (26) (Fig. 5A). Electroretinography was analyzed using two representative points: i) The a-wave, which is the initial negative deflection representing photoreceptor function, and ii) the b-wave, which is the positive deflection representing bipolar, amacrine and Muller cell functions (37). The mean of amplitudes of the a- and b-waves showed no significant difference between the two groups, which together indicated no toxicity in the functional aspects of the retina (37) (Fig. 5B).

In agreement with previous results, there was no difference in histological integrity between different groups according to H&E staining (Fig. 5C and D). TUNEL assay revealed similar results, with only three to six TUNEL-positive cells, indicating the presence of only a few apoptotic cells in both injection and control groups. These results demonstrated that BB-Cl-amidine had a markedly low toxicity profile, which supported its potential for clinical translation (Fig. 5E and F). Collectively, the current study revealed that RB1 deficiency upregulated PADI2 expression by E2F activation, and that PADI2 inhibition significantly attenuated cancer cell growth via p-ATK inactivation, which resulted in cancer cell death (Fig. 5G).

Discussion

Previous studies have reported that PADI2 is upregulated in various cancer types and is involved in tumorigenesis (17,20). Therefore, PADI2 is considered a potential therapeutic target for cancer treatment. However, the role of PADI2 in retinoblastoma has not been elucidated to date. The present study determined that PADI2 functioned as an oncogenic driver in the tumorigenesis of retinoblastoma *in vitro* and *in vivo*. Since there are numerous binding sites for Sp1 in the promoter of PADI2, and activated Sp1 increases the expression of PADI2 in retinoblastoma (10), it was confirmed in the current study that PADI2 was highly expressed in representative retinoblastoma cell lines and samples from patients with retinoblastoma. Since the expression of PADI2 is low in human retinal pigment epithelium cells and PADI2 inhibition has little effect on the viability of these cells, PADI2 has clinical importance as a specific therapeutic target in retinoblastoma.

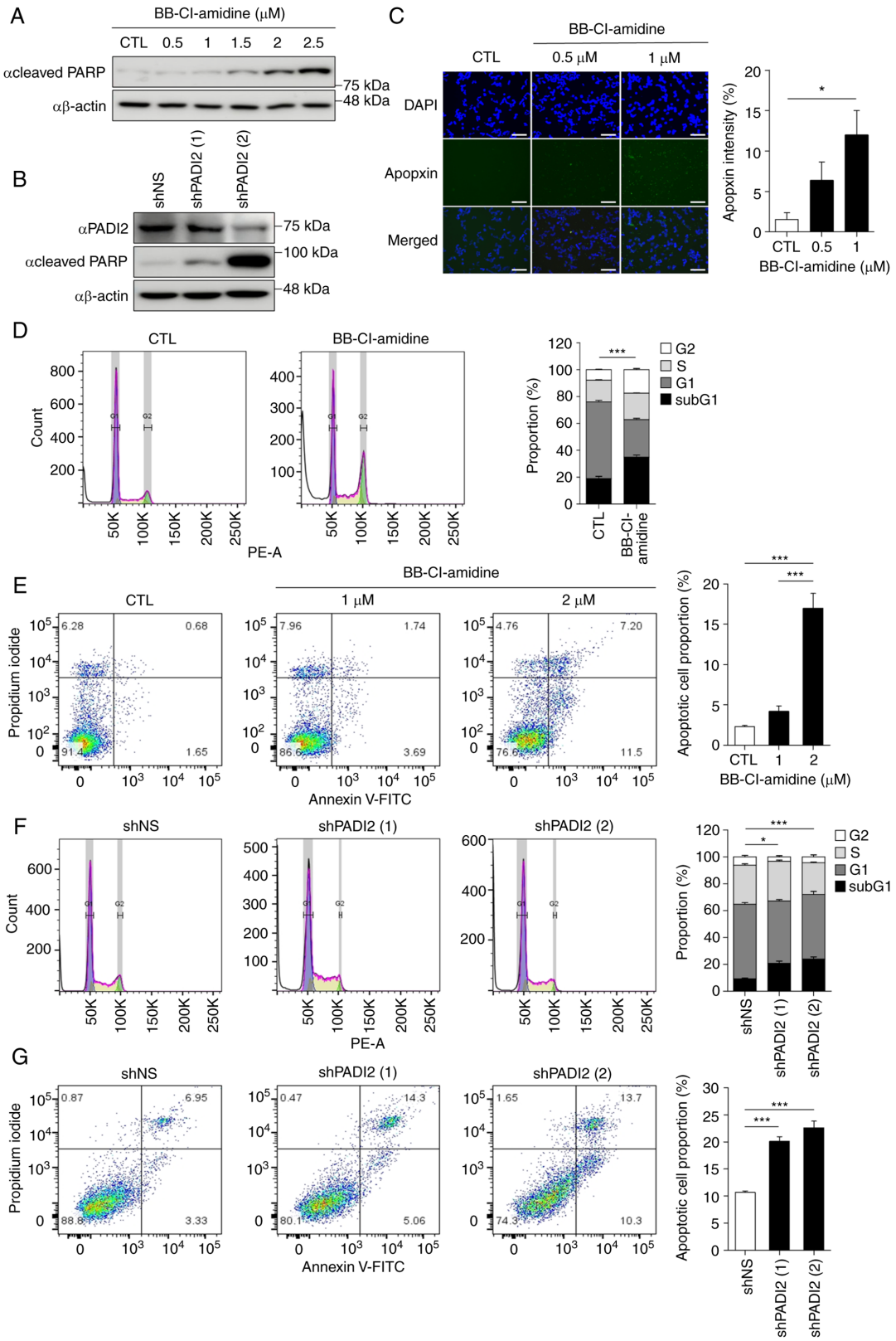

Figure 3. PADI2 inhibition induces cancer cell death *in vitro*. (A and B) Expression of cleaved poly (ADP-ribose) polymerase protein in (A) Y79 cells treated with DMSO and BB-Cl-amidine for 48 h in a dose-dependent manner or (B) control and PADI2-depleted Y79 cells, as determined by western blotting assay. (C) Apoptosis-positive areas in Y79 cells treated with DMSO and BB-Cl-amidine (0.5 and 1 μM) for 48 h were analyzed by Apoptosis/Necrosis Assay Kit. Apopxin Green$^+$ indicates the apoptotic cells. Representative immunostaining images (left) and graphs of Apopxin Green intensity (right) are shown (magnification, x20). Scale bar, 125 μm (n=5). (D) Distributions of the cell cycle at sub-G_1 (black), G_1 (dark grey), S (bright grey) and G_2 (white) phases in Y79 cells treated with DMSO and 2 μM BB-Cl-amidine for 48 h, as determined by flow cytometry (n=4). (E) Proportions of total apoptotic cells in Y79 cells treated with DMSO and 2 μM BB-Cl-amidine for 48 h, as determined by annexin V-FITC/PI staining (n=4). (F) Distribution of the cell cycle in control and PADI2-depleted Y79 cells, as evaluated by flow cytometry (n=4). (G) Proportion of total apoptotic cells in control and PADI2-depleted Y79 cells, as determined by annexin V-FITC/PI staining (n=4). (D-G) Statistical graphs (top) and representative cell distribution results (bottom) are shown. Bars indicate SEM. *P≤0.05 and ***P≤0.001, as determined by (C, E and G) one-way ANOVA with post-hoc Bonferroni test and (D and F) two-way ANOVA with post-hoc Bonferroni test. PADI2, protein arginine deiminase II; PI, propidium iodide.

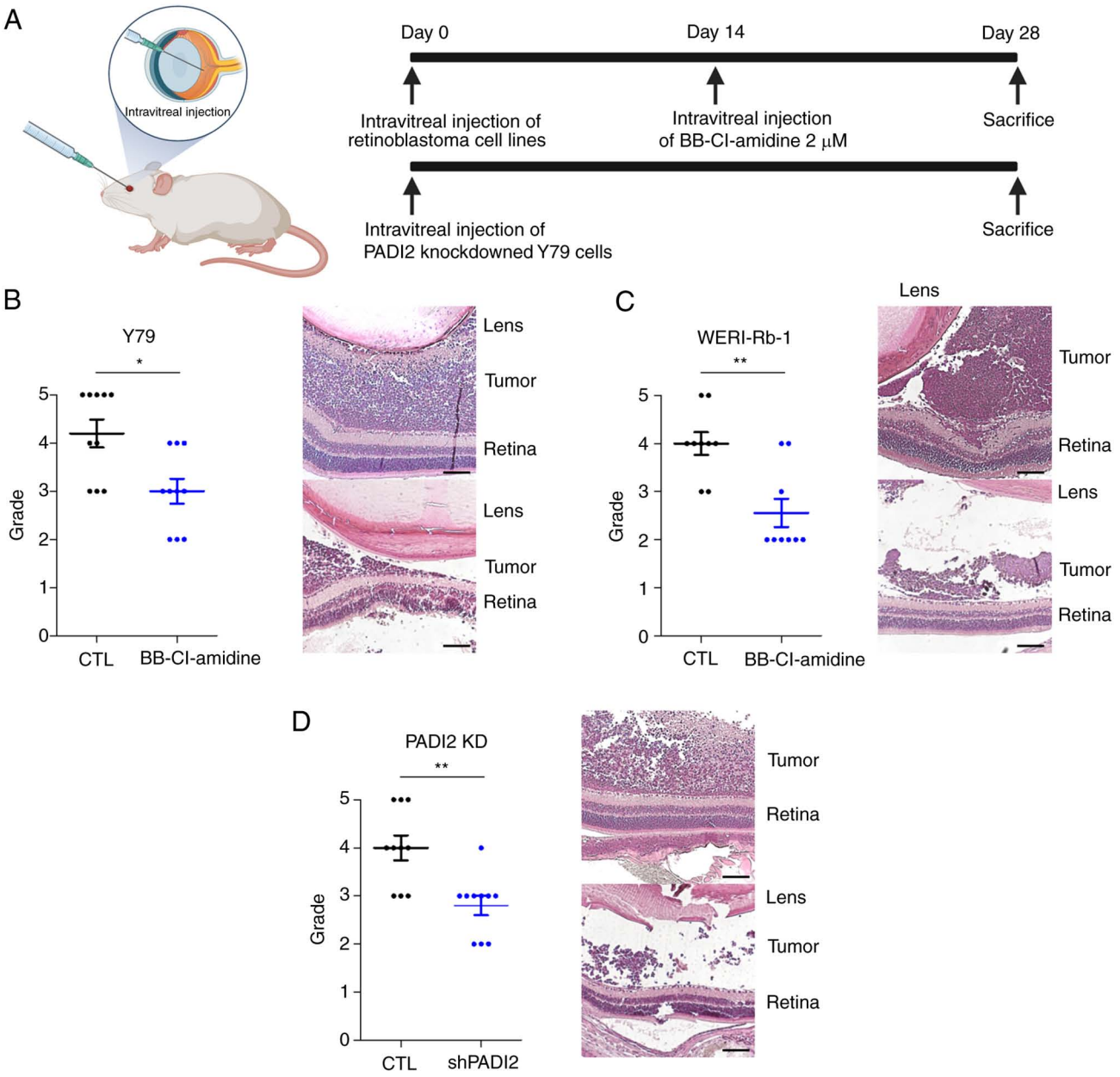

Figure 4. PADI2 inhibition suppresses tumor growth *in vivo*. (A) Timeline of PADI2 inhibition in an orthotopic transplantation mouse model. (B-D) BB-Cl-amidine, a PADI2 chemical inhibitor, suppressed tumor growth. (B) Y79 (n=10) and (C) WERI-Rb-1 cells (n=9) were injected intravitreally. BB-Cl-amidine was intravitreally injected after 14 days, followed by euthanasia and evaluation after 14 additional days. (D) PADI2 was knocked down in Y79 cells using shRNA (n=10). Intravitreal injection was followed by euthanasia and evaluation after 28 days. Graphs of visual grading of tumors (left) and representative hematoxylin and eosin staining images (right) are shown (magnification, x40). Scale bar, 100 μm. Bars indicate SEM. *P≤0.05 and **P≤0.01, as determined by (B-D) U-Mann Whitney test. PADI2, protein arginine deiminase II; sh-, short hairpin.

The current study demonstrated that the modulation of PADI2 occurred in two directions in retinoblastoma. First, upregulation of PADI2 enhanced the growth of retinoblastoma. It was observed that the proliferation of Y79 cells was suppressed, and p-AKT was downregulated by treatment with BB-Cl-amidine, a potent inhibitor of PADI2 (38). In addition, it was confirmed that PADI2-knockdown Y79 cells exhibited similar characteristics as cells subjected to treatment with BB-Cl-amidine. It was first suggested that BB-Cl-amidine was a selective inhibitor of PADI2 with an antitumor effect in retinoblastoma. In a recent study, p-AKT was reported to be involved in retinoblastoma proliferation by inactivating methyltransferase-like 3, which plays a role in an epigenetic modification of RNA and is associated with the development of tumors (34). Therefore, further studies on the involvement of specific epigenetic regulators or downstream target genes affected by the axis of PADI2-AKT activation are needed. Next, PADI2 inhibition was found to induce cancer cell death in the present study. It was observed that PADI2 inactivation elevated cleaved PARP expression and apoptotic signatures in retinoblastoma. These results suggested that PADI2 inhibition may be able to simultaneously control cell proliferation and death, suggesting that it may be an important regulator of retinoblastoma.

Retinoblastoma has been primarily regarded as a genetic disease induced by mutations or deletions in the *RB1* gene.

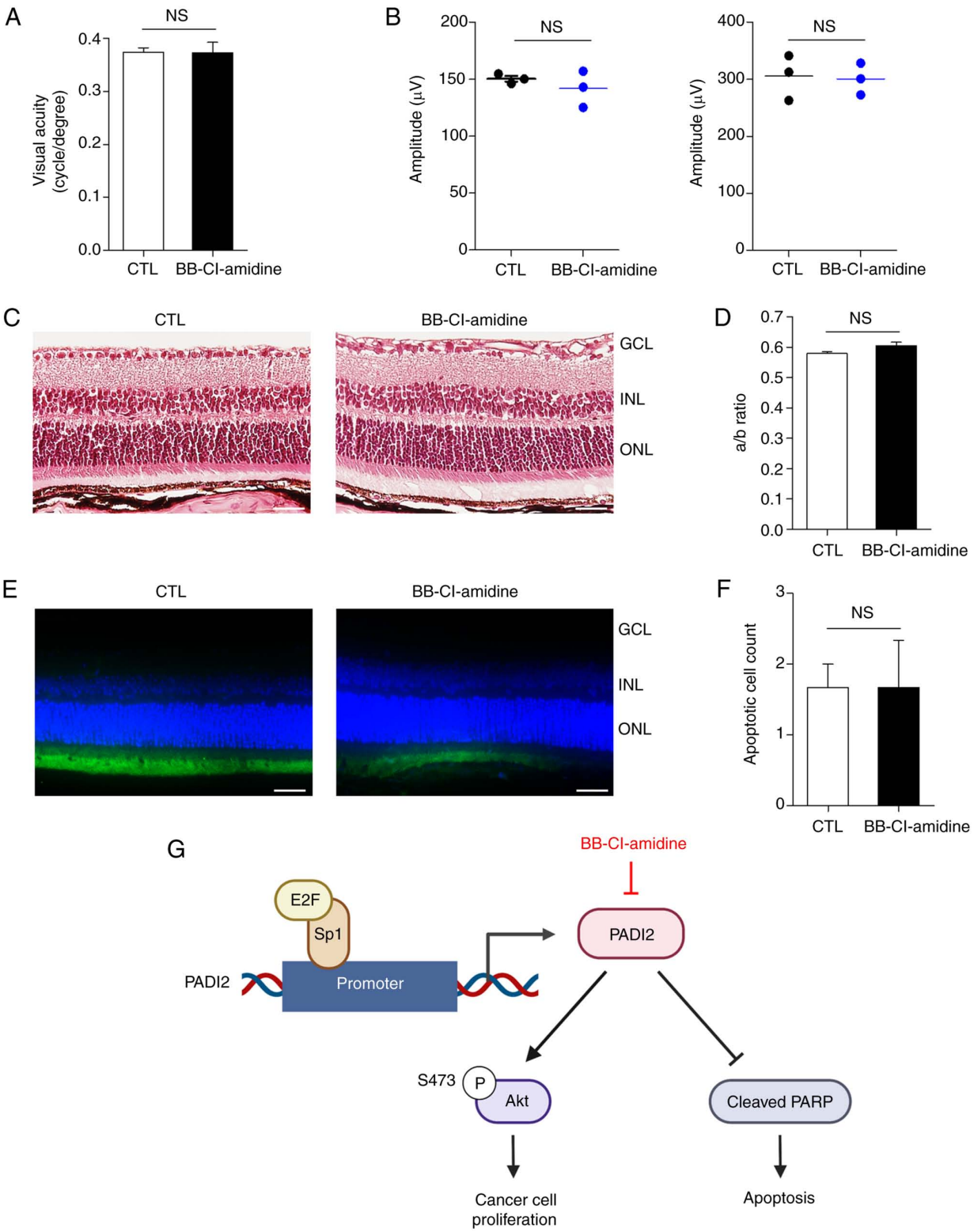

Figure 5. Toxicity profiles of PADI2 inhibitor. Evaluation of histology and function of retina after intravitreal injection of PBS and 2 μM BB-Cl-amidine in mice. (A) Visual acuity was evaluated through optomotor response in different groups. (B) The a-wave (left) and b-wave (right) were measured by electroretinography in different groups. (C and D) (C) Representative images (magnification, x200) and (D) quantitative analyses of hematoxylin and eosin staining of various groups. (E and F) (E) Representative images (magnification, x200) and (F) quantitative analyses of TUNEL assay. The number of apoptotic cells did not show a statistically significant difference between the groups. (G) Schematic of summary. Scale bar, 50 μm (n=3). Bars represent SEM. NS, not significant, as determined by unpaired Student's t-test.

Various treatments targeting *RB1* have been explored, but treatment limitations have not yet been overcome. Therefore, it is imperative to consider epigenetic factors that are beyond the limits of genetic factors. The current study showed that enzymatic inhibition or ablation of PADI2 could be a crucial epigenetic therapy for retinoblastoma. It is necessary to

develop and optimize a potent inhibitor of PADI2 or design a delivery method that can selectively eliminate PADI2 using CRISPR/Cas9 in cancer tissues in an attempt to overcome the limitations of the existing treatments.

In conclusion, the present study demonstrated the oncogenic function of PADI2 in retinoblastoma. PADI2 expression was enhanced by activating the binding of Sp1 to free E2F. Treatment with a selective inhibitor of PADI2 and knockdown of PADI2 expression led to suppression of cell proliferation via p-AKT inactivation and cancer cell death *in vitro*. *In vivo* experiments also showed that PADI2 inhibition significantly weakened tumorigenic effects. These results provide fundamental considerations for developing a novel therapeutic strategy for retinoblastoma.

Acknowledgements

Not applicable.

Funding

The present study was supported by the Basic Science Research Program (grant nos. NRF-2020R1C1C1010489 and NRF-2022R1A2C1003768), the National Research Foundation of Korea (funded by the Korean government; grant no. 2022R1A2C2010940) and Korea University Medical Center (grant no. K2210331).

Availability of data and materials

The datasets used and/or analyzed during the current study are available from the corresponding author on reasonable request.

Authors' contributions

SK and YKS participated in formal analysis, investigation, data curation, methodology, writing of the original draft of the manuscript, reviewing and editing of the article and confirm the authenticity of all the raw data. CSC participated in data curation and investigation. HJK participated in methodology, writing, reviewing and editing the manuscript. SF participated in methodology, reviewing and editing the manuscript. DHJ participated in conceptualization, data curation, formal analysis, methodology, writing of the original draft of the manuscript, and reviewing and editing of the article. HK participated in conceptualization, formal analysis, data curation, supervision, methodology, writing of the original draft of the manuscript, and reviewing and editing of the article. All authors read and approved the final manuscript.

Ethics approval and consent to participate

All animal experiments were performed with the approval (approval no. SNU-220512-3) of the Institutional Research Ethics Committee of Seoul National University College (Seoul, Korea).

Patient consent for publication

Not applicable.

Competing interests

The authors declare that they have no competing interests.

References

1. Dimaras H, Corson TW, Cobrinik D, White A, Zhao J, Munier FL, Abramson DH, Shields CL and Chantada GL: Retinoblastoma. Nat Rev Dis Primers 1: 15021, 2015.
2. Giacinti C and Giordano A: RB and cell cycle progression. Oncogene 25: 5220-5227, 2006.
3. Vermeulen K, Van Bockstaele DR and Berneman ZN: The cell cycle: A review of regulation, deregulation and therapeutic targets in cancer. Cell Prolif 36: 131-149, 2003.
4. Park SJ, Woo SJ and Park KH: Incidence of retinoblastoma and survival rate of retinoblastoma patients in Korea using the Korean national cancer registry database (1993-2010). Invest Ophthalmol Vis Sci 55: 2816-2821, 2014.
5. Jung EH, Kim JH, Kim JY, Jo DH and Yu YS: Outcomes of proton beam radiation therapy for retinoblastoma with vitreous seeds. J Pediatr Hematol Oncol 40: 569-573, 2018.
6. Moon J, Choi SH, Lee MJ, Jo DH, Park UC, Yoon SO, Woo SJ and Oh JY: Ocular surface complications of local anticancer drugs for treatment of ocular tumors. Ocul Surf 19: 16-30, 2021.
7. Karlseder J, Rotheneder H and Wintersberger E: Interaction of Sp1 with the growth- and cell cycle-regulated transcription factor E2F. Mol Cell Biol 16: 1659-1667, 1996.
8. Lin SY, Black AR, Kostic D, Pajovic S, Hoover CN and Azizkhan JC: Cell cycle-regulated association of E2F1 and Sp1 is related to their functional interaction. Mol Cell Biol 16: 1668-1675, 1996.
9. Rotheneder H, Geymayer S and Haidweger E: Transcription factors of the Sp1 family: Interaction with E2F and regulation of the murine thymidine kinase promoter. J Mol Biol 293: 1005-1015, 1999.
10. Dong S, Kojima T, Shiraiwa M, Méchin MC, Chavanas S, Serre G, Simon M, Kawada A and Takahara H: Regulation of the expression of peptidylarginine deiminase type II gene (PADI2) in human keratinocytes involves Sp1 and Sp3 transcription factors. J Invest Dermatol 124: 1026-1033, 2005.
11. Nagai T, Matsueda Y, Tomita T, Yoshikawa H and Hirohata S: The expression of mRNA for peptidylarginine deiminase type 2 and type 4 in bone marrow CD34+ cells in rheumatoid arthritis. Clin Exp Rheumatol 36: 248-253, 2018.
12. Ishigami A, Ohsawa T, Asaga H, Akiyama K, Kuramoto M and Maruyama N: Human peptidylarginine deiminase type II: Molecular cloning, gene organization, and expression in human skin. Arch Biochem Biophys 407: 25-31, 2002.
13. Wang H, Xu B, Zhang X, Zheng Y, Zhao Y and Chang X: PADI2 gene confers susceptibility to breast cancer and plays tumorigenic role via ACSL4, BINC3 and CA9 signaling. Cancer Cell Int 16: 61, 2016.
14. Clancy KW, Russell AM, Subramanian V, Nguyen H, Qian Y, Campbell RM and Thompson PR: Citrullination/methylation crosstalk on histone H3 regulates ER-target gene transcription. ACS Chem Biol 12: 1691-1702, 2017.
15. Liu L, Zhang Z, Zhang G, Wang T, Ma Y and Guo W: Down-regulation of PADI2 prevents proliferation and epithelial-mesenchymal transition in ovarian cancer through inhibiting JAK2/STAT3 pathway in vitro and in vivo, alone or in combination with Olaparib. J Transl Med 18: 357, 2020.
16. Sharma P, Lioutas A, Fernandez-Fuentes N, Quilez J, Carbonell-Caballero J, Wright RHG, Vona CD, Dily FL, Schüller R, Eick D, *et al*: Arginine citrullination at the C-terminal domain controls RNA polymerase II transcription. Mol Cell 73: 84-96 e87, 2019.
17. Wang L, Song G, Zhang X, Feng T, Pan J, Chen W, Yang M, Bai X, Pang Y, Yu J, *et al*: PADI2-mediated citrullination promotes prostate cancer progression. Cancer Res 77: 5755-5768, 2017.
18. Guertin MJ, Zhang X, Anguish L, Kim S, Varticovski L, Lis JT, Hager GL and Coonrod SA: Targeted H3R26 deimination specifically facilitates estrogen receptor binding by modifying nucleosome structure. PLoS Genet 10: e1004613, 2014.
19. Horibata S, Rogers KE, Sadegh D, Anguish LJ, McElwee JL, Shah P, Thompson PR and Coonrod SA: Role of peptidylarginine deiminase 2 (PAD2) in mammary carcinoma cell migration. BMC Cancer 17: 378, 2017.

20. Xue T, Liu X, Zhang M, Qiukai E, Liu S, Zou M, Li Y, Ma Z, Han Y, Thompson P and Zhang X: PADI2-catalyzed MEK1 citrullination activates ERK1/2 and promotes IGF2BP1-mediated SOX2 mRNA stability in endometrial cancer. Adv Sci (Weinh) 8: 2002831, 2021.
21. Jo DH, Kim JH, Cho CS, Cho YL, Jun HO, Yu YS, Min JK and Kim JH: STAT3 inhibition suppresses proliferation of retinoblastoma through down-regulation of positive feedback loop of STAT3/miR-17-92 clusters. Oncotarget 5: 11513-11525, 2014.
22. Jo DH, Lee S, Bak E, Cho CS, Han YT, Kim K, Suh YG and Kim JH: Antitumor activity of novel signal transducer and activator of transcription 3 inhibitors on retinoblastoma. Mol Pharmacol 100: 63-72, 2021.
23. Cho CS, Jo DH, Kim JH and Kim JH: Establishment and characterization of carboplatin-resistant retinoblastoma cell lines. Mol Cells 45: 729-737, 2022.
24. Khokhlova ON, Tukhovskaya EA, Kravchenko IN, Sadovnikova ES, Pakhomova IA, Kalabina EA, Lobanov AV, Shaykhutdinova ER, Ismailova AM and Murashev AN: Using tiletamine-zolazepam-xylazine anesthesia compared to CO(2)-inhalation for terminal clinical chemistry, hematology, and coagulation analysis in mice. J Pharmacol Toxicol Methods 84: 11-19, 2017.
25. Jo DH, Lee K, Kim JH, Jun HO, Kim Y, Cho YL, Yu YS, Min JK and Kim JH: L1 increases adhesion-mediated proliferation and chemoresistance of retinoblastoma. Oncotarget 8: 15441-15452, 2017.
26. Jang H, Jo DH, Cho CS, Shin JH, Seo JH, Yu G, Gopalappa R, Kim D, Cho SR, Kim JH and Kim HH: Application of prime editing to the correction of mutations and phenotypes in adult mice with liver and eye diseases. Nat Biomed Eng 6: 181-194, 2022.
27. Xu H, Koch P, Chen M, Lau A, Reid DM and Forrester JV: A clinical grading system for retinal inflammation in the chronic model of experimental autoimmune uveoretinitis using digital fundus images. Exp Eye Res 87: 319-326, 2008.
28. Chen M, Copland DA, Zhao J, Liu J, Forrester JV, Dick AD and Xu H: Persistent inflammation subverts thrombospondin-1-induced regulation of retinal angiogenesis and is driven by CCR2 ligation. Am J Pathol 180: 235-245, 2012.
29. Testa JR and Bellacosa A: AKT plays a central role in tumorigenesis. Proc Natl Acad Sci USA 98: 10983-10985, 2001.
30. Liu W, Bagaitkar J and Watabe K: Roles of AKT signal in breast cancer. Front Biosci 12: 4011-4019, 2007.
31. Shukla S, Maclennan GT, Hartman DJ, Fu P, Resnick MI and Gupta S: Activation of PI3K-Akt signaling pathway promotes prostate cancer cell invasion. Int J Cancer 121: 1424-1432, 2007.
32. Fu R, Yang P, Wu HL, Li ZW and Li ZY: GRP78 secreted by colon cancer cells facilitates cell proliferation via PI3K/Akt signaling. Asian Pac J Cancer Prev 15: 7245-7249, 2014.
33. Yan X, Wu S, Liu Q and Zhang J: RRS1 promotes retinoblastoma cell proliferation and invasion via activating the AKT/mTOR signaling pathway. Biomed Res Int 2020: 2420437, 2020.
34. Zhang H, Zhang P, Long C, Ma X, Huang H, Kuang X, Du H, Tang H, Ling X and Ning J: m(6)A methyltransferase METTL3 promotes retinoblastoma progression via PI3K/AKT/mTOR pathway. J Cell Mol Med 24: 12368-12378, 2020.
35. Bao XY, Sun M, Peng TT and Han DM: TRIB3 promotes proliferation, migration, and invasion of retinoblastoma cells by activating the AKT/mTOR signaling pathway. Cancer Biomark 31: 307-315, 2021.
36. Diefenbach J and Bürkle A: Introduction to poly(ADP-ribose) metabolism. Cell Mol Life Sci 62: 721-730, 2005.
37. Creel DJ: Electroretinograms. Handb Clin Neurol 160: 481-493, 2019.
38. Monreal MT, Rebak AS, Massarenti L, Mondal S, Šenolt L, Ødum N, Nielsen ML, Thompson PR, Nielsen CH and Damgaard D: Applicability of small-molecule inhibitors in the study of peptidyl arginine deiminase 2 (PAD2) and PAD4. Front Immunol 12: 716250, 2021.